

## Protein Side-Chain Dynamics Observed by Solution- and Solid-State NMR: Comparative Analysis of Methyl $^2\text{H}$ Relaxation Data

Bernd Reif,<sup>†,\*</sup> Yi Xue,<sup>‡</sup> Vipin Agarwal,<sup>†</sup> Maria S. Pavlova,<sup>‡</sup> Maggy Hologne,<sup>†</sup> Anne Diehl,<sup>†</sup> Yaroslav E. Ryabov,<sup>‡</sup> and Nikolai R. Skrynnikov<sup>‡,\*</sup>

Forschungsinstitut für Molekulare Pharmakologie (FMP), Robert-Rössle-Str. 10, 13125 Berlin, Germany, and Department of Chemistry, Purdue University, 560 Oval Drive, West Lafayette, Indiana 47907-2084

Received April 21, 2006; E-mail: nikolai@purdue.edu

It is well-known that protein structures in solution are generally very similar to those found in hydrated crystals. Relatively little has been done, however, to compare the internal dynamics of proteins in solution and in solids.<sup>1–4</sup> The progress in this area has been hampered by the lack of high-resolution solid-state NMR techniques. With recent advances in solid-state spectroscopy, it became possible to obtain dynamic information on a per-residue basis using uniformly labeled protein samples.<sup>5,6</sup> In this communication we demonstrate how solid-state relaxation data collected in this manner can be analyzed jointly with solution-state data.

Side-chain methyl groups that dominate the protein hydrophobic core are among the most interesting dynamic entities in the protein. A convenient probe of methyl dynamics is provided by deuterium relaxation.  $^2\text{H}$  relaxes via a quadrupolar mechanism, with the quadrupolar tensor essentially invariant among different methyl sites.<sup>7</sup> The relaxation is driven mainly by the fast spinning of the methyl groups, so that the  $T_1^{-1}$  rates are approximately proportional to the corresponding correlation times,  $\tau_f^{\text{Me}}$  (Figure S1, Supporting Information (SI)). The rates vary substantially from one site to another since  $\tau_f^{\text{Me}}$  are sensitive to the details of the van der Waals environment.<sup>8–10</sup>

To compare methyl dynamics in solid and solution NMR samples we conducted a series of relaxation measurements on the SH3 domain from chicken  $\alpha$ -spectrin. Protein was expressed in *E. coli* by growing cells in 100%  $\text{D}_2\text{O}$ , using 3-[60%  $^2\text{H}$ ,  $^{13}\text{C}$ ]-labeled pyruvate as the sole carbon source.<sup>11</sup> Pulse sequences used to measure solution-state  $^2\text{H}$   $T_1$ ,  $T_{1\rho}$ ,  $T_{1zz}$  and  $^{15}\text{N}$   $T_1$ ,  $T_{1\rho}$ , NOE were adapted, with minor alterations, from the literature.<sup>12,13</sup> A newly developed pulse sequence for solid-state  $^2\text{H}$   $T_1$  measurements is shown in Figure S2. The data were collected at 10 °C, 600 MHz, 24 kHz MAS frequency.

Two additional samples,  $u(^2\text{H}, ^{13}\text{C}, ^{15}\text{N})$  and  $u(^{13}\text{C}, ^{15}\text{N}), 50\% ^2\text{H}$ , were prepared for solid and solution experiments, respectively, using glucose as a carbon source. All measurements were repeated with these samples; in the case of solids, the recently reported  $^2\text{H}$   $T_1$  pulse sequence was used.<sup>6</sup> The quality of the spectra for uniformly  $^{13}\text{C}$ -labeled material was somewhat lower; therefore, only the data from Ala and Ile- $\delta$  methyls (which are poorly labeled in the pyruvate-based sample) were retained from this data set.

The representative relaxation curves from methyl  $^2\text{H}$   $T_1$  measurements are shown in Figure S3 and the correlation between the solid- and solution-state rates is presented in Figure 1a. While Figure 1a establishes a useful point of reference, one should bear in mind that the solution  $T_1^{-1}$  rates contain substantial contribution from the overall tumbling. To deal with this contribution, we determined the rotational diffusion tensor of  $\alpha$ -spc-SH3 using  $^{15}\text{N}$  relaxation data.<sup>13,14</sup> We further interpreted the set of solution-state methyl  $^2\text{H}$

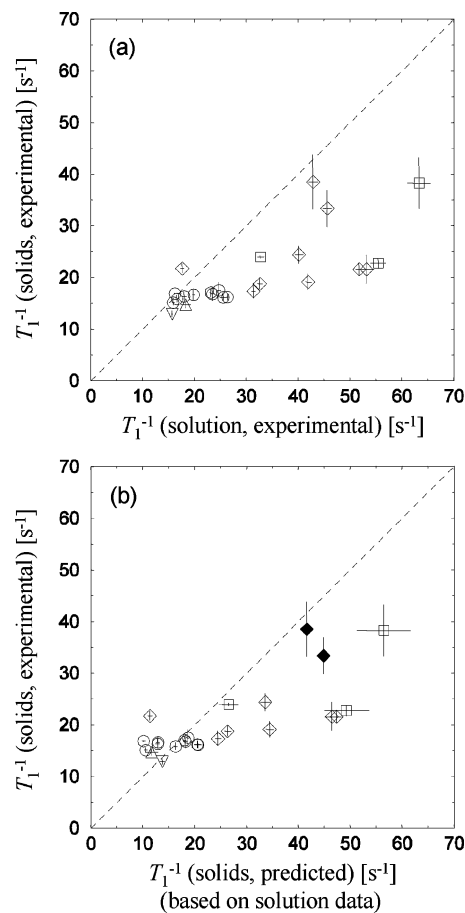


**Figure 1.**  $^2\text{H}$   $T_1^{-1}$  relaxation rates for 24 methyl sites in  $\alpha$ -spectrin SH3 domain. Solid-state rates are plotted against (a) respective solution-state rates, and (b) predicted solid-state rates, where the prediction is based on the analyses of solution data. Methyls are labeled as  $\square$  (Ala),  $\diamond$  (Val),  $\triangle$  (Ile- $\gamma$ ),  $\nabla$  (Ile- $\delta$ ), and  $\circ$  (Leu). Two Val-23 sites are indicated by filled symbols. The correlation coefficient for the data in panel b is  $r = 0.76$ .

rates,  $T_1^{-1}$ ,  $T_{1\rho}^{-1}$ , and  $T_{1zz}^{-1}$ , in terms of the Lipari–Szabo model<sup>15,16</sup>

$$J(\omega) = \left(\frac{1}{9}\right)S^2 \frac{\tau_R}{1 + \omega^2 \tau_R^2} + \left(1 - \left(\frac{1}{9}\right)S^2\right) \frac{\tau}{1 + \omega^2 \tau^2}$$

$$\tau^{-1} = \tau_f^{-1} + \tau_R^{-1} \quad (1)$$

The fast-motion correlation time,  $\tau_f$ , and its associated order parameter,  $(1/9)S^2$ , were treated as fitting variables, whereas  $\tau_R$  was fixed according to  $^{15}\text{N}$  data,  $\tau_R = 6.0$  ns.<sup>17</sup> The time  $\tau_f$  is mainly determined by the methyl rotation,  $\tau_f^{\text{Me}}$ , but also reflects backbone and side-chain librations as well as fast rotameric jumps (provided that these jumps connect substantially populated rotameric states).<sup>18–20</sup>

<sup>†</sup> Forschungsinstitut für Molekulare Pharmakologie.

<sup>‡</sup> Purdue University.

In using the two-parameter Lipari–Szabo model we neglected the possible effect of slower ( $\sim 1$  to 10 ns) rotameric transitions in methyl-bearing side chains. It has been previously demonstrated that these transitions play a role only for a small fraction of all residues.<sup>21,22</sup> Spectral density mapping<sup>23</sup> confirmed that eq 1 adequately describes all methyls with a notable exception of Val-23 (see Figure S4). Our previous crystallographic studies and  $^2\text{H}$  MAS line shape analyses showed that the side chain of Val-23 samples multiple conformations in solids.<sup>6,24</sup>

The best-fit  $S^2$  and  $\tau_f$  values obtained from the analysis of the solution-state data were used to calculate rotation-free spectral densities

$$J(\omega) = \left(1 - \left(\frac{1}{9}\right)S^2\right) \frac{\tau_f}{1 + \omega^2\tau_f^2} \quad (2)$$

and subsequently predict solid-state  $^2\text{H}$   $T_1^{-1}$  relaxation rates. Those predicted rates are correlated with the experimental solid-state rates in Figure 1b.

Figure 1b demonstrates a substantial degree of similarity between methyl dynamics in solids and solutions. The solid-state rates, however, tend to be more homogeneous and lower than expected. We attribute this effect to  $^2\text{H}$ – $^2\text{H}$  spin diffusion which occurs under the conditions of the MAS experiment.<sup>25</sup> In brief, the interchange of magnetization between different  $^2\text{H}$  sites tends to equalize the observable relaxation rates. In particular, partial averaging takes place between rapidly relaxing methyls and slowly relaxing “rigid” sites. The resulting trend toward lower and more uniform apparent rates is especially visible for several Ala and Val methyls where the expected rates are higher than average (points on the right side of the plot).

On the basis of the formalism by Gan and Robyr,<sup>26</sup> we conducted a series of numerical simulations to evaluate the effects of  $^2\text{H}$  spin diffusion on the measured solid-state relaxation rates (see SI for details). It has been estimated, for instance, that the coupling between  $3\text{-}^2\text{H}^\alpha$  and  $^2\text{H}^\beta$  in the valine side chain typically causes a drop of  $0\text{--}4\text{ s}^{-1}$  in the measurable methyl relaxation rate (depending on chemical shift offset between the two spins and on methyl  $\tau_f$ ). At the same time, this coupling increases the effective relaxation rate of  $^2\text{H}^\beta$ , in agreement with our previous data.<sup>27</sup> The methyls play, therefore, a familiar role of “relaxation sinks”.<sup>28</sup> We also simulated spin diffusion between two proximal methyl groups belonging to different residues. The changes in apparent relaxation rates up to  $4\text{ s}^{-1}$  have been found in these simulations. Although accurate analysis of spin diffusion in the extended spin network is not feasible, our simulations clearly account for the trends observed in Figure 1b.

After making an allowance for the spin diffusion, our data suggest that there is a high degree of similarity between methyl dynamics in solid and in solution. Indeed, in small globular proteins such as the SH3 domain the hydrophobic core is encapsulated in a fairly rigid scaffold. In this sequestered environment, side chain motion (and particularly the rotation of methyl groups) does not depend on whether the sample is classified as liquid or solid, so long as the protein remains in contact with a “thermal bath” represented by a large pool of fluid water.

Since methyl  $^2\text{H}$   $T_1^{-1}$  relaxation rates are controlled by rapid methyl spinning, these data are well suited to demonstrate the similarity between solution- and solid-state dynamics. Once the

similarity is established, it opens up some interesting possibilities for future studies. In backbone, for example, fast local dynamics ( $\tau_f$ ) is relatively inefficient in causing relaxation so that slow forms of internal motion ( $\tau_s$ ) can play a significant role.<sup>29</sup> Of special interest is the situation where solution data are sensitive to  $\tau_f$  and  $\tau_R$ , while solid-state data are sensitive to  $\tau_f$  and  $\tau_s$ . In this case, the combination of the two methods can be particularly useful, providing valuable information about slow collective motions.<sup>30,31</sup>

**Acknowledgment.** We thank Ad Bax, Dennis Torchia, and Beat Meier for drawing our attention to deuterium spin diffusion.

**Supporting Information Available:** MD simulations of methyl  $^2\text{H}$   $T_1$  data; solid-state pulse sequence for measuring  $^2\text{H}$   $T_1$  relaxation; solid- and solution-state relaxation curves; spectral density profiles; table of  $S^2$  and  $\tau_f$  values; simulations of  $^2\text{H}$ – $^2\text{H}$  spin diffusion in MAS experiment. This material is available free of charge via the Internet at <http://pubs.acs.org>.

## References

- (1) Sparks, S. W.; Cole, H. B. R.; Torchia, D. A.; Young, P. E. *Chem. Scr.* **1989**, *29A*, 31–38.
- (2) Tamura, A.; Matsushita, M.; Naito, A.; Kojima, S.; Miura, K. I.; Akasaka, K. *Protein Sci.* **1996**, *5* (1), 127–139.
- (3) Rozovsky, S.; Jögl, G.; Tong, L.; McDermott, A. E. *J. Mol. Biol.* **2001**, *310* (1), 271–280.
- (4) Rozovsky, S.; McDermott, A. E. *J. Mol. Biol.* **2001**, *310* (1), 259–270.
- (5) Giraud, N.; Böckmann, A.; Lesage, A.; Penin, F.; Blackledge, M.; Emsley, L. *J. Am. Chem. Soc.* **2004**, *126* (37), 11422–11423.
- (6) Hologne, M.; Faelber, K.; Diehl, A.; Reif, B. *J. Am. Chem. Soc.* **2005**, *127* (32), 11208–11209.
- (7) Mittermaier, A.; Kay, L. E. *J. Am. Chem. Soc.* **1999**, *121* (45), 10608–10613.
- (8) Hoatun, G. L.; Vold, R. L.  *$^2\text{H}$  NMR Spectroscopy of Solids and Liquid Crystals*. In *NMR Basic Principles and Progress*; Diehl, P.; Fluck, E.; Gunther, H.; Kosfeld, R., Seelig, J., Eds.; Springer-Verlag: Berlin, 1994; Vol. 32, pp 1–65.
- (9) Chatfield, D. C.; Augsten, A.; D’Cunha, C. *J. Biomol. NMR* **2004**, *29* (3), 377–385.
- (10) Mittermaier, A.; Kay, L. E. *Protein Sci.* **2004**, *13* (4), 1088–1099.
- (11) Lee, A. L.; Urbauer, J. L.; Wand, A. J. *J. Biomol. NMR* **1997**, *9* (4), 437–440.
- (12) Millet, O.; Muhandiram, D. R.; Skrynnikov, N. R.; Kay, L. E. *J. Am. Chem. Soc.* **2002**, *124* (22), 6439–6448.
- (13) Farrow, N. A.; Muhandiram, R.; Singer, A. U.; Pascal, S. M.; Kay, C. M.; Gish, G.; Shoelson, S. E.; Pawson, T.; Forman-Kay, J. D.; Kay, L. E. *Biochemistry* **1994**, *33* (19), 5984–6003.
- (14) Lee, L. K.; Rance, M.; Chazin, W. J.; Palmer, A. G. *J. Biomol. NMR* **1997**, *9* (3), 287–298.
- (15) Lipari, G.; Szabo, A. *J. Am. Chem. Soc.* **1982**, *104* (17), 4546–4559.
- (16) Kay, L. E.; Torchia, D. A. *J. Magn. Reson.* **1991**, *95* (3), 536–547.
- (17) In the final analysis, eq 1 was modified to account for anisotropic tumbling of the protein. The asymmetry parameter for  $\alpha\text{-spc-SH3}$  is 1.23.
- (18) Chatfield, D. C.; Szabo, A.; Brooks, B. R. *J. Am. Chem. Soc.* **1998**, *120* (21), 5301–5311.
- (19) Best, R. B.; Clarke, J.; Karplus, M. *J. Mol. Biol.* **2005**, *349* (1), 185–203.
- (20) Hu, H.; Hermans, J.; Lee, A. L. *J. Biomol. NMR* **2005**, *32* (2), 151–162.
- (21) Skrynnikov, N. R.; Millet, O.; Kay, L. E. *J. Am. Chem. Soc.* **2002**, *124* (22), 6449–6460.
- (22) Tang, C.; Iwahara, J.; Clore, G. *J. Biomol. NMR* **2005**, *33* (2), 105–121.
- (23) Peng, J. W.; Wagner, G. *J. Magn. Reson.* **1992**, *98* (2), 308–332.
- (24) Chevelkov, V.; Faelber, K.; Diehl, A.; Heinemann, U.; Oschkinat, H.; Reif, B. *J. Biomol. NMR* **2005**, *31* (4), 295–310.
- (25) Alla, M.; Eckman, R.; Pines, A. *Chem. Phys. Lett.* **1980**, *71*, (1), 148–151.
- (26) Gan, Z. H.; Robyr, P. *Mol. Phys.* **1998**, *95* (6), 1143–1152.
- (27) Hologne, M.; Chen, Z. J.; Reif, B. *J. Magn. Reson.* **2006**, *179* (1), 20–28.
- (28) Kalk, A.; Berendsen, H. J. C. *J. Magn. Reson.* **1976**, *24* (3), 343–366.
- (29) Mack, J. W.; Usha, M. G.; Long, J.; Griffin, R. G.; Wittebort, R. J. *Biopolymers* **2000**, *53* (1), 9–18.
- (30) Bouvignies, G.; Bernado, P.; Meier, S.; Cho, K.; Grzesiek, S.; Brüschweiler, R.; Blackledge, M. *Proc. Natl. Acad. Sci. U.S.A.* **2005**, *102* (39), 13885–13890.
- (31) Lakomek, N. A.; Farès, C.; Becker, S.; Carlomagno, T.; Meiler, J.; Griesinger, C. *Angew. Chem., Int. Ed.* **2005**, *44* (47), 7776–7778.

JA062808A

## Supporting Information

### **Protein side-chain dynamics observed by solution- and solid-state NMR: comparative analysis of methyl $^2\text{H}$ relaxation data.**

Bernd Reif<sup>†\*</sup>, Yi Xue<sup>‡</sup>, Vipin Agarwal<sup>†</sup>, Maria S. Pavlova<sup>‡</sup>, Maggy Hologne<sup>†</sup>, Anne Diehl<sup>†</sup>,  
Yaroslav E. Ryabov<sup>‡</sup>, Nikolai R. Skrynnikov<sup>‡\*</sup>

<sup>†</sup> *Forschungsinstitut für Molekulare Pharmakologie (FMP), Robert-Rössle-Str. 10, 13125 Berlin, Germany*

<sup>‡</sup> *Department of Chemistry, Purdue University, 560 Oval Dr., W. Lafayette, IN 47907-2084, USA*

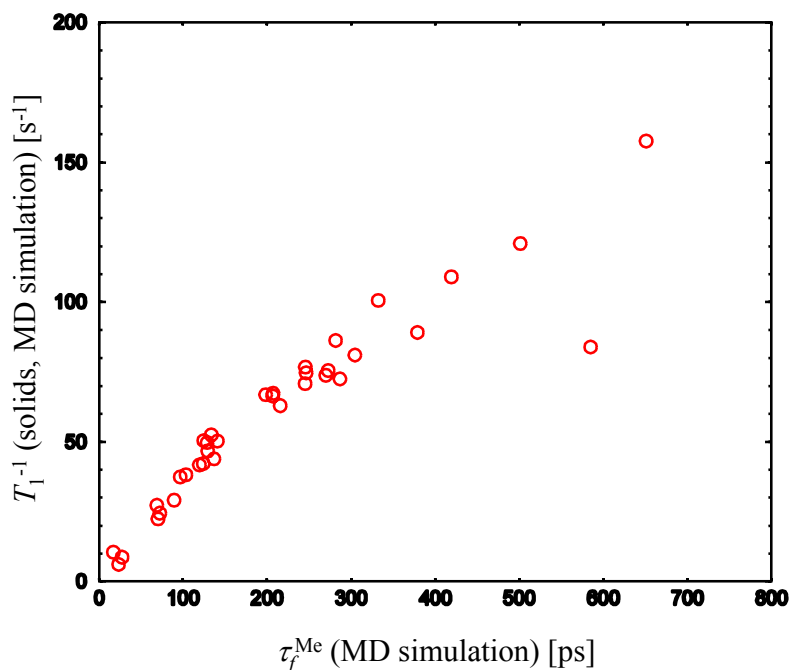


**Figure S1.** Simulated solid-state methyl  $^2\text{H}$   $T_1^{-1}$  rates as a function of methyl rotation correlation times,  $\tau_f^{\text{Me}}$ . Based on a 40-ns-long MD trajectory<sup>1</sup> of a 63-residue protein L<sup>2</sup> recorded with the program NAMD.<sup>3</sup> The rates for multiple methyl sites were computed assuming axially symmetric deuterium quadrupolar tensor with the principal axis along the CH bond and the magnitude  $e^2qQ/h = 167$  kHz.<sup>4</sup>

The correlation functions were evaluated as  $g(\tau) = (4\pi/5) \sum_{q=-2}^2 \overline{Y_{2q}(\Omega(t)) Y_{2q}^*(\Omega(t+\tau)) - Y_{2q}(\Omega(t)) Y_{2q}^*(\Omega(t))}$  and multiplied by the window function,  $\exp(-\tau/100 \text{ ns})$ , in order to eliminate unreasonably long tails which are not supported by the length of the MD trajectory.

To derive  $\tau_f^{\text{Me}}$  values, we extracted from the MD trajectory the time dependence of the dihedral angle associated with methyl rotation,  $\chi(t)$ . This dependence was used as an input to generate a correlation function  $g^{\text{Me}}(\tau)$  (assuming rigid tetrahedral geometry of the methyl group). The result was then fitted to the expression  $g^{\text{Me}}(\tau) = (1/9) + (1 - (1/9)) \exp(-\tau/\tau_f^{\text{Me}})$ , thus arriving to the best-fit value of  $\tau_f^{\text{Me}}$  which characterizes the spinning of the methyl group.

It is known that molecular dynamics employing CHARMM force field tends to overestimate  $\tau_f^{\text{Me}}$ .<sup>5</sup> In particular, residues with  $\tau_f^{\text{Me}} > 500$  ps (points on the right side of the plot) suffer from poor sampling of methyl rotation and are generally unreliable. Otherwise, a tight correlation between the simulated  $T_1^{-1}$  rates and  $\tau_f^{\text{Me}}$  is obvious in the plot.

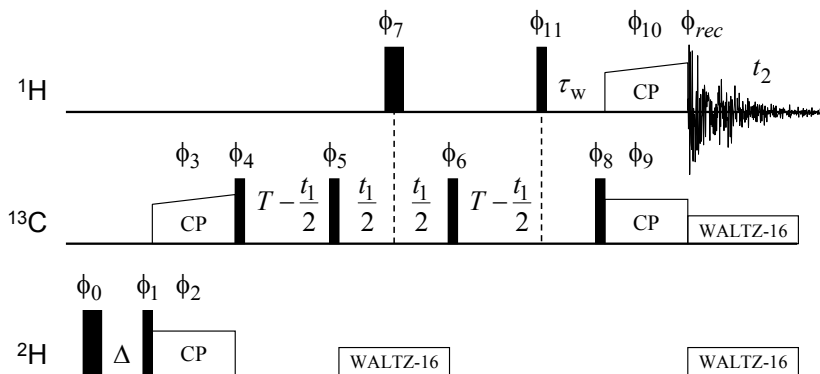


**Figure S2.** A solid-state NMR experiment for measuring  ${}^2\text{H}$   $T_1^{-1}$  relaxation in methyl groups. The sequence was designed for application to the samples that are selectively  ${}^{13}\text{C}$ -labeled in the methyl position and contain both  ${}^1\text{H}$  and  ${}^2\text{H}$  spins within a given methyl group. Narrow (wide) pulses were applied with a flip angle of  $90^\circ$  ( $180^\circ$ ). The  $rf$  carriers were set at 4.94 (HDO line) and 20.8 for  ${}^1\text{H}$  and  ${}^{13}\text{C}$ , respectively. The hard pulses were applied with the power levels of 60, 41, and 71 kHz for  ${}^1\text{H}$ ,  ${}^{13}\text{C}$ , and  ${}^2\text{H}$ , respectively. WALTZ-16 decoupling<sup>7</sup> on the  ${}^{13}\text{C}$  and  ${}^2\text{H}$  channels employed a 2.5 and 2.8 kHz field, respectively. For the first CP element, the  ${}^2\text{H}$  field was 64 kHz and the  ${}^{13}\text{C}$  field was matched at (-1) spinning sideband, with the span of the linear ramp 10 kHz.<sup>8,9</sup> For the second CP element, the  ${}^{13}\text{C}$  field was 16.5 kHz and the  ${}^1\text{H}$  field was matched at (+1) spinning sideband, with the span of the linear ramp 12 kHz. The delays used were:  $\tau_{CP}({}^2\text{H}, {}^{13}\text{C}) = 4.6$  ms,  $\tau_{CP}({}^{13}\text{C}, {}^1\text{H}) = 2$  ms,  $T = 65$  ms,  $\tau_w = 20$  ms, and  $\Delta = [0, 5, 20, 35, 70, 100, 250]$  ms. The recycling delay between the two consecutive scans was 0.5 s. The spectral widths in the  ${}^{13}\text{C}$  and  ${}^1\text{H}$  dimensions were 3100 and 60000 Hz, respectively (the latter was extended to avoid folding of the spinning sidebands in the spectrum). The phase cycle was  $\phi_0 = y$ ,  $\phi_1 = (x, -x)$ ,  $\phi_2 = 16(-y)16(y)$ ,  $\phi_3 = 32(x)32(-x)$ ,  $\phi_4 = 32(y)32(-y)$ ,  $\phi_5 = 32(-x)32(x)$ ,  $\phi_6 = x$ ,  $\phi_7 = (x, -x)$ ,  $\phi_8 = 4(x)4(-x)$ ,  $\phi_9 = y$ ,  $\phi_{10} = 2(x, x, -x, -x)2(y, y, -y, -y)$ ,  $\phi_{11} = 16(y)16(x)16(-y)16(-x)$ ,  $\phi_{rec} = P, \bar{P}, \bar{P}, P$ , where  $P = (x, -x, -x, x)(-x, x, x, -x)(y, -y, -y, y)(-y, y, y, -y)$ . Quadrature detection in  $t_1$  was achieved by States-TPPI<sup>10</sup> of  $\phi_6$ . The sample spinning rate was 24 kHz.

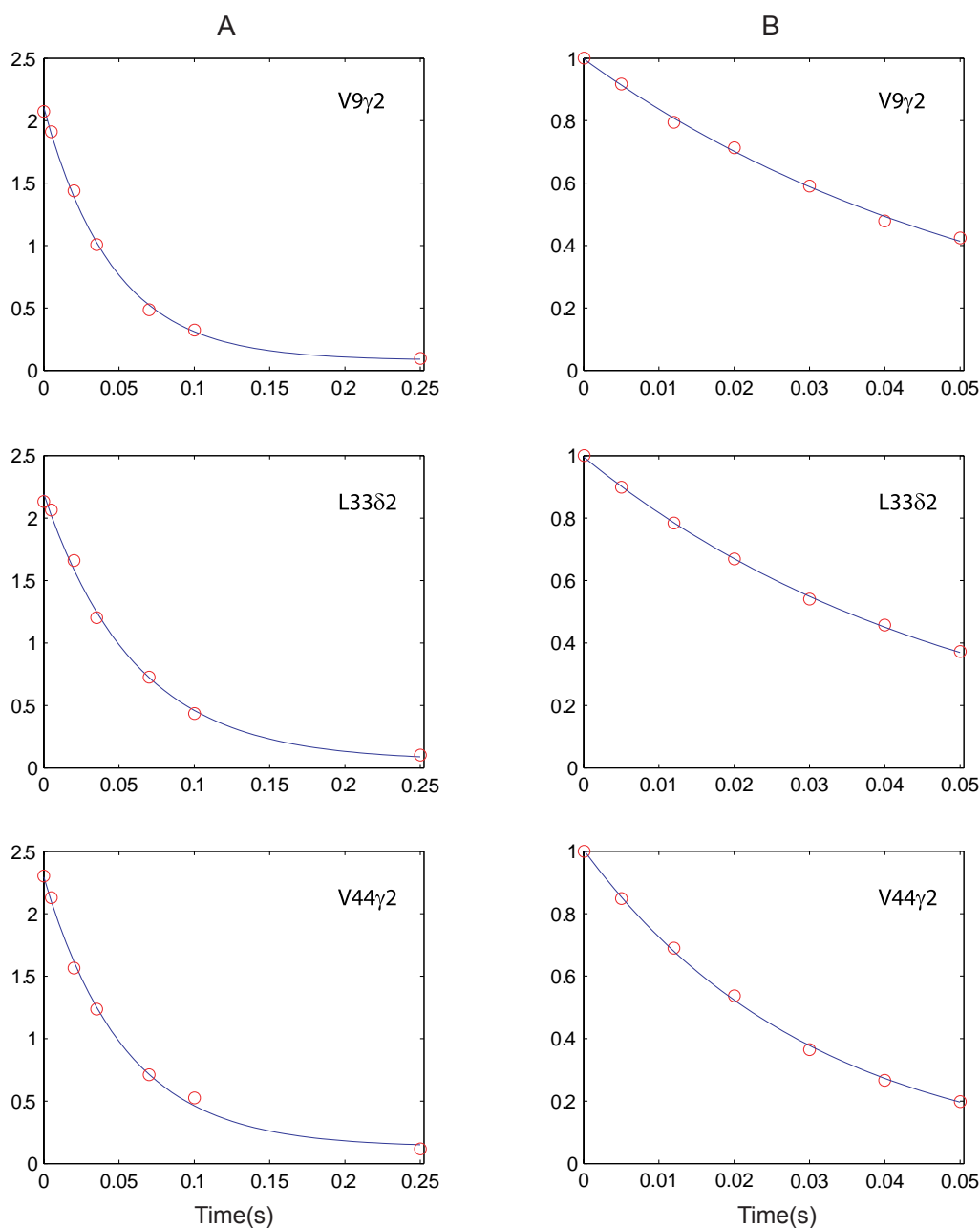


**Figure S3.** Methyl  $^2\text{H}$   $T_1^{-1}$  relaxation profiles as recorded in solid (left column) and solution (right column) experiments. The three methyls in this figure illustrate a typical quality of solid-state data (specifically, the data were sorted according to the exponential fitting *rmsd* and three residues were picked from the middle of the list). For comparison, the solution data for these same residues are presented in the right column. The data were recorded in 20 and 60 hours for solution- and solid-state experiments, respectively. All measurements were conducted at 600 MHz, 10 °C (in the case of the solid-state experiments, sample heating has been taken into consideration). The sample conditions for solution-state experiment were 1.5 mM protein, pH 3.5 (unbuffered), 90:10  $\text{H}_2\text{O}:\text{D}_2\text{O}$ . For solid studies, the protein was precipitated by means of pH shift as described previously.<sup>11, 12</sup> The peak intensities in the spectra were integrated using nlinLS<sup>13</sup> and fitted according to  $(I_0 - I_\infty) \exp(-\Delta/T_1) + I_\infty$  (solid) or  $I_0 \exp(-\Delta/T_1)$  (solution).

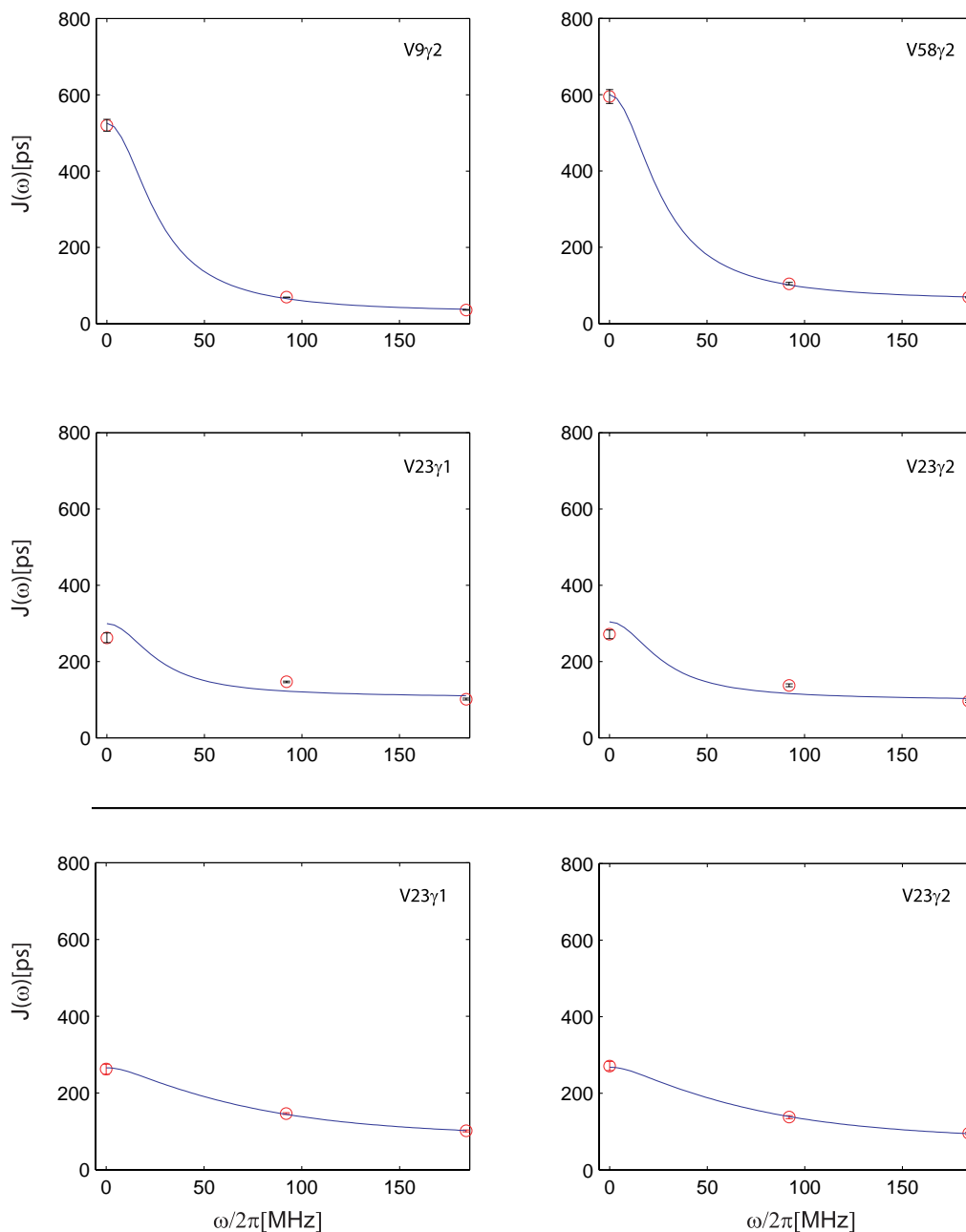


**Figure S4.** Spectral density mapping for selected methyl sites in the  $\alpha$ -spectrin SH3 domain. The three spectral densities,  $J(0)$ ,  $J(\omega_D)$ , and  $J(2\omega_D)$ , have been extracted from  $T_1^{-1}$ ,  $T_{1\rho}^{-1}$ , and  $T_{1zz}^{-1}$  (quadrupolar order) rates measured in solution. The (small) error bars have been generated using the Monte-Carlo procedure. The curves have been generated by fitting  $T_1^{-1}$ ,  $T_{1\rho}^{-1}$ , and  $T_{1zz}^{-1}$  to Eq. 1 (adapted for anisotropically tumbling molecule). Quadrupolar coupling constants were assumed to be uniform,  $e^2qQ/h = 167$  kHz.<sup>4</sup> The top two panels illustrate the typical quality of the fit (specifically, we sorted the data according to the fitting *rmsd* and picked a pair of residues from the middle of the list). The agreement throughout the data set is excellent with the exception of Val-23 (middle row) where the correlation function is affected by rotameric jumps on the time scale of several nanoseconds.

The data from Val-23 were also interpreted using a more sophisticated model (bottom row).

Specifically, the data from both Val-23 methyls (six experimentally measured rates) were fitted to the extended Lipari-Szabo type model.<sup>14, 15</sup> In doing so, fast-motion variables  $S^2$  and  $\tau_f$  were fitted for each methyl group individually, whereas slow-motion parameters  $S_s^2$  and  $\tau_s$  were common for both sites. Good fits were obtained in the range of  $S_s^2 = 0.00 - 0.15$ , with respective time scales  $\tau_s = 4.0 - 1.7$  ns (the curves shown in the bottom portion of the plot correspond to  $S_s^2 = 0.10$ ,  $\tau_s = 2.8$  ns). These results point toward extensive averaging with regard to  $\chi_1$ . The solid-state  $T_1^{-1}$  rates predicted for Val-23 in this analysis were only 1-2  $s^{-1}$  lower than the values obtained on the basis of the simple two-parameter model. Therefore, we choose not to correct the results shown in Fig. 1b.



Methyl group	$S^2$	$\tau_f$ (ps)
A11	$0.90 \pm 0.03$	$135 \pm 12$
A55	$0.95 \pm 0.04$	$157 \pm 14$
A56	$0.84 \pm 0.02$	$71 \pm 5$
V9 $\gamma$ 1	$0.82 \pm 0.03$	$90 \pm 2$
V9 $\gamma$ 2	$0.75 \pm 0.03$	$30 \pm 1$
V23 $\gamma$ 1 <sup>(a)</sup>	$0.29 \pm 0.03$	$114 \pm 2$
V23 $\gamma$ 2 <sup>(b)</sup>	$0.31 \pm 0.02$	$106 \pm 3$
V44 $\gamma$ 1	$0.87 \pm 0.04$	$93 \pm 2$
V44 $\gamma$ 2	$0.84 \pm 0.01$	$71 \pm 2$
V46 $\gamma$ 1	$0.63 \pm 0.02$	$65 \pm 1$
V46 $\gamma$ 2	$0.64 \pm 0.01$	$58 \pm 1$
V53 $\gamma$ 1	$0.90 \pm 0.04$	$127 \pm 4$
V53 $\gamma$ 2	$0.66 \pm 0.03$	$126 \pm 2$
V58 $\gamma$ 1	$0.70 \pm 0.03$	$61 \pm 1$
V58 $\gamma$ 2	$0.82 \pm 0.03$	$66 \pm 1$
I30 $\gamma$	$0.81 \pm 0.05$	$31 \pm 3$
I30 $\delta$	$0.30 \pm 0.04$	$35 \pm 1$
L8 $\delta$ 1	$0.62 \pm 0.02$	$27 \pm 1$
L8 $\delta$ 2	$0.71 \pm 0.02$	$49 \pm 1$
L10 $\delta$ 1	$0.70 \pm 0.03$	$9 \pm 1$
L10 $\delta$ 2	$0.61 \pm 0.02$	$47 \pm 1$
L12 $\delta$ 1	$0.69 \pm 0.03$	$27 \pm 1$
L12 $\delta$ 2	$0.72 \pm 0.06$	$54 \pm 1$
L31 $\delta$ 1	$0.29 \pm 0.02$	$89 \pm 1$
L31 $\delta$ 2	$0.34 \pm 0.02$	$43 \pm 1$
L33 $\delta$ 1	$0.66 \pm 0.02$	$34 \pm 1$
L33 $\delta$ 2	$0.79 \pm 0.02$	$34 \pm 1$
L34 $\delta$ 1	$0.62 \pm 0.02$	$47 \pm 1$
L34 $\delta$ 2	$0.62 \pm 0.03$	$54 \pm 2$
L61 $\delta$ 1	$0.45 \pm 0.01$	$33 \pm 1$
L61 $\delta$ 2	$0.43 \pm 0.01$	$41 \pm 1$

**Table S1.** Order parameters,  $S^2$ , and correlation times,  $\tau_f$ , obtained from the Lipari-Szabo analysis of methyl  $^2\text{H}$   $T_1^{-1}$ ,  $T_{1\rho}^{-1}$ , and  $T_{1zz}^{-1}$  relaxation data in solution. The data are from the pyruvate-based (selectively  $^{13}\text{C}$ -labeled) sample, except in the case of the Ala and Ile- $\delta$  sites where the data are from the glucose-based (uniformly  $^{13}\text{C}$ -labeled) sample.

(a) The extended analysis, see Fig. S4, yields  $S^2 = 0.69 - 0.87$  and  $\tau_f = 92 - 80$  ps

(b) The extended analysis, see Fig. S4, yields  $S^2 = 0.76 - 0.92$  and  $\tau_f = 82 - 69$  ps

## Effects of $^2\text{H}$ - $^2\text{H}$ spin diffusion on measurements of deuterium $T_1^{-1}$ relaxation rates.

Dipolar-driven spin diffusion in deuterated molecules under MAS conditions was first described by Alla, Eckman, and Pines.<sup>16</sup> These authors also pointed out that spin-diffusion can compromise  $^2\text{H}$   $T_1^{-1}$  measurements. In brief, the interchange of magnetization between different  $^2\text{H}$  sites tends to equalize the observable relaxation rates. Notably, partial averaging takes place between rapidly relaxing methyls and the rest of the deuterium spins which relax slowly.

In order to simulate this effect, we took advantage of the formalism developed by Gan and Robyr for the system of two coupled spins  $I=1$ ,  $S=1$ .<sup>17</sup> The starting geometry was that of the aliphatic chain, with spin  $I$  representing methyl and spin  $S$  representing proximal methine or methylene. For example, in the case of valine side chain the treatment was formulated for  $^2\text{H}^\gamma$  and  $^2\text{H}^\beta$  spins. The quadrupolar tensor for  $^2\text{H}^\beta$  was assumed to be axially symmetric with unique axis along  $\text{H}^\beta\text{-C}^\beta$  bond and the amplitude  $e^2qQ/h = 167$  kHz.<sup>4</sup> For the methyl group, the partially averaged tensor has the symmetry axis along  $\text{C}^\beta\text{-C}^\gamma$  bond and the amplitude  $(1/3)e^2qQ/h = 55.7$  kHz. The quadrupolar relaxation rates were simulated for the methyl group assuming  $\tau_f = 80$  ps,  $\omega_0^H / 2\pi = 600$  MHz. The chemical shift difference between  $^2\text{H}^\gamma$  and  $^2\text{H}^\beta$  was taken to be 1.17 ppm according to the average value reported in the BMRB database.<sup>18</sup> The sample spinning rate was assumed to be 24 kHz, same as in the experimental study.

The treatment was formulated using the product operator basis. Since none of the terms in the master equation (including the dipolar flip-flop term and quadrupolar relaxation) can induce coupling between  $\Delta M=0, 1, 2$ , etc. manifolds, only  $\Delta M=0$  manifold has been retained to analyze longitudinal relaxation. This manifold is spanned by:

$$\{E, I_z, 3I_z^2 - 2E\} \otimes \{E, S_z, 3S_z^2 - 2E\} \quad (\text{S1.1})$$

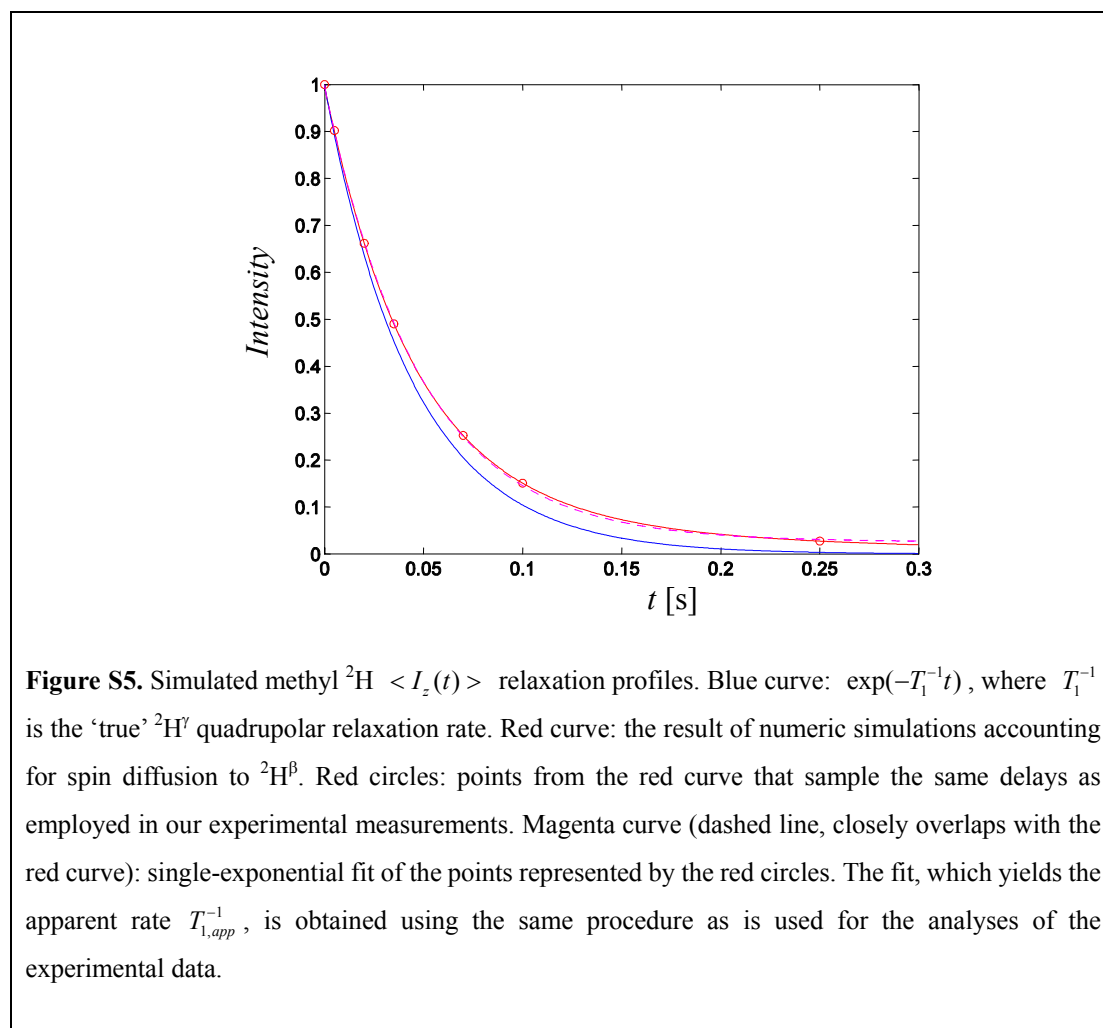
$$\{I_+, I_+I_z + I_zI_+\} \otimes \{S_-, S_-S_z + S_zS_-\} + \text{conjugate operators} \quad (\text{S1.2})$$

$$\{I_+^2\} \otimes \{S_-^2\} + \text{conjugate operators} \quad (\text{S1.3})$$

for the total of 19 operators, including identity. The relaxation rates for these modes, including two-spin modes, can be calculated in a straightforward fashion. In doing so we assumed that methyl spin  $I$  is relaxed via the quadrupolar mechanism modulated by methyl rotation. Spin  $S$ , on the other hand, represents the ‘rigid’ deuterium site for which quadrupolar relaxation is known to be inefficient (the rate was set to zero in our simulations).<sup>16</sup> With only one relaxation channel to consider, the set of the quadrupolar relaxation rates for the modes Eq. (S1) is given by familiar expressions.<sup>19</sup>

The dipolar Liouvillian matrix was evaluated according to Gan and Robyr in the basis of fictitious spin-1/2 and spin-1 operators.<sup>17</sup> It was subsequently transformed into the basis Eq. (S1). The elements of the matrix connecting  $S_z$  and  $3S_z^2 - 2E$  with the rest of the modes,  $(S_z \hat{H}_{dip} B_i)$  and  $([3S_z^2 - 2E] \hat{H}_{dip} B_i)$ , have been multiplied by 3 to account for the presence of three equivalent  $^2\text{H}$  spins in the methyl group. The Liouvillian matrix was then combined with the relaxation matrix and the spin evolution was computed beginning with the initial conditions  $I_z(0) = S_z(0) = 1$ , corresponding to the non-selective deuterium relaxation measurement.

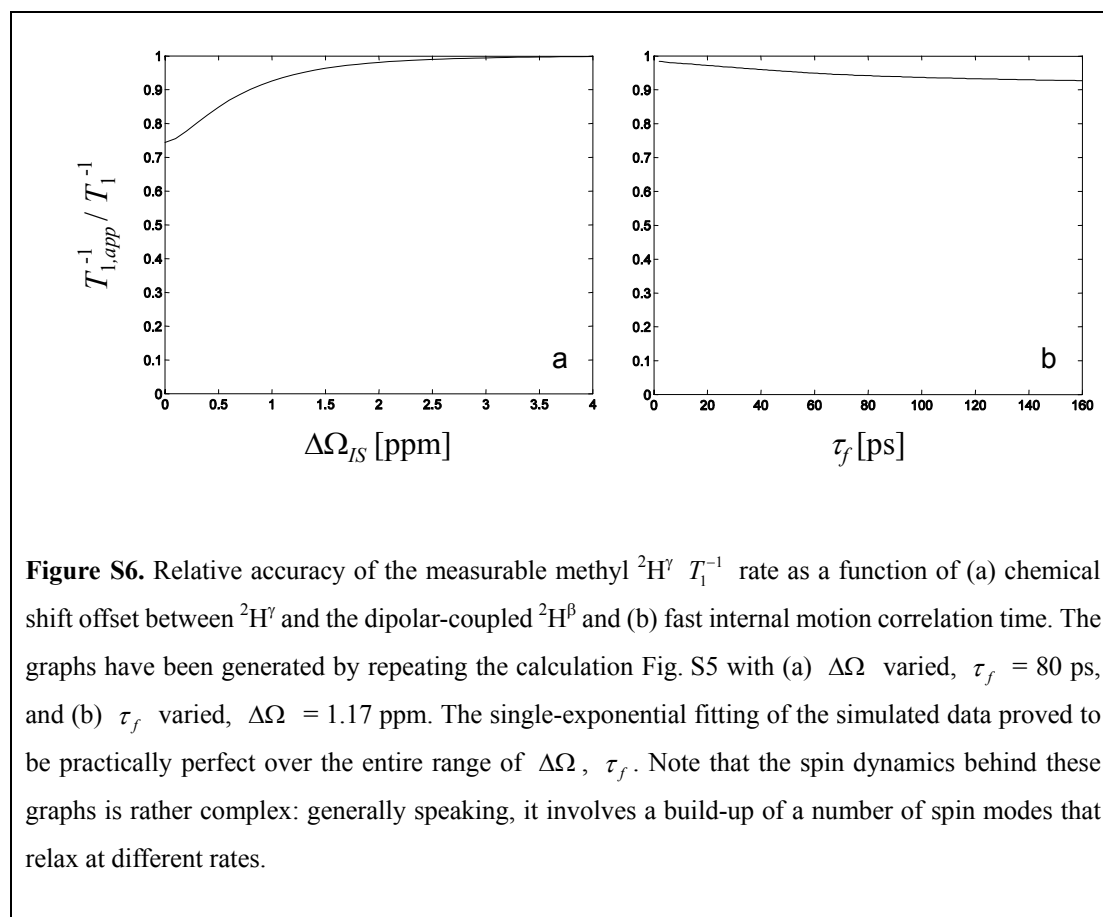
The decay curve  $I_z(t)$  obtained in this manner is representative of a microcrystal with certain specific orientation relative to the rotor frame. To calculate the response from the powder sample, this calculation has been repeated for 900 different microcrystal orientations which provide optimal sampling of the unit sphere<sup>20</sup> (the convergence of the integration procedure was confirmed by reproducing Fig. 2 in the work by Gan and Robyr<sup>17</sup>). The resulting  $I_z(t)$  curves were then added with the prescribed weights<sup>20</sup> and the net decay profile  $\langle I_z(t) \rangle$  was thus generated.



The results of this simulation are presented in Fig. S5. As expected, the decay of the methyl magnetization is slowed down due to the spin diffusion involving slowly relaxing  $^2\text{H}^\beta$  (cf. red and blue curves). The apparent methyl rate drops by 6% relative to the target value. Conversely, the simulated decay of  $^2\text{H}^\beta$  (not shown) is entirely due to the presence of the ‘‘methyl sink’’ nearby. The simulated apparent rates,  $T_{1,app}^{-1}(^2\text{H}_3^\gamma) = 21 \text{ s}^{-1}$  and  $T_{1,app}^{-1}(^2\text{H}^\beta) = 5 \text{ s}^{-1}$ , are in agreement with the recent measurements on u- $^2\text{H}$  NAc-Val sample performed under similar (although not identical) conditions.<sup>21</sup>

Of note, the effect of  $^2\text{H}$ - $^2\text{H}$  spin diffusion is strongly dependent on the chemical shift offset between the two deuterium spins. This effect is illustrated in Fig. S6a. According to conventional wisdom, the dipolar flip-flop term cannot effectively couple two spin states with large energy separation.

As a result, spin diffusion effects disappear if the difference in chemical shifts becomes sufficiently large,  $>3$  ppm. On the other hand, when chemical shifts are degenerate spin diffusion leads to thorough mixing of magnetization. When the mixing occurs between three methyl  $^2\text{H}$  spins with the relaxation rate  $T_1^{-1}$  and a single proximal  $^2\text{H}$  spin with the relaxation rate 0, the apparent decay rate is  $T_{1,app}^{-1} = (3/4)T_1^{-1}$  ( $y$ -axis intercept in Fig. S6a). An important corollary of this result is that Ala and Thr, that typically show large  $\Delta\Omega$ , are less likely to be affected by spin diffusion than Leu and Ile.<sup>22</sup>



Another instructive dependence is plotted in Fig. S6b. It turns out that methyl sites with long  $\tau_f$  and, accordingly, with high quadrupolar relaxation rates are more prone to spin-diffusion effects. This effect can be explained in a familiar fashion: broadening of  $^2\text{H}$  transitions facilitates polarization transfer in the system with a chemical shift offset. This is relevant for the Ala and Val side chains that tend to have higher relaxation rates (cf. Tab. S1).

One additional source of  $^2\text{H}$  broadening is dipolar interaction with proximal protons. While our glucose-derived samples are uniformly deuterated, pyruvate-derived samples contain protons in methyl positions. A simple way to account for the presence of protons is to add an empirical decay constant to the description of the two-spin deuterium system.<sup>17</sup> Based on the proton linewidth, we estimated this decay constant to be on the order of ca.  $15\text{ s}^{-1}$ . This generic number was subsequently added to the auto-relaxation rates of the coherences Eqs. (S1.2, S1.3) and the simulations of Fig. S5 were repeated. The resulting enhancement of the spin diffusion was rather insignificant (additional 1% drop in the

apparent methyl  $^2\text{H}$  relaxation rate). We note that the role of protons in this context is similar to that in proton-driven  $^{13}\text{C}$ - $^{13}\text{C}$  spin diffusion.<sup>23</sup>

In addition to the intra-residue processes, we also considered the possibility of spin diffusion between different methyl groups. As a test case, we selected Val53  $\gamma_2$  and Val58  $\gamma_1$  that form a very close contact in the structure of the SH3 domain (effective distance after averaging over fast methyl rotations 3.5 Å).<sup>24</sup> The correlation times  $\tau_f$  for the two respective methyl groups were set to 126 and 61 ps, in accordance to the solution-state data. The chemical shift offset  $\Delta\Omega$ , as observed in the spectrum, was 0.25 ppm. To account for the presence of three equivalent deuterons in each methyl group, the elements of the dipolar Liouvillian connecting  $I_z$  and  $3I_z^2 - 2E$  with the rest of the modes were multiplied by 3 (same for the elements connecting  $S_z$  and  $3S_z^2 - 2E$  with the rest of the modes).

The simulations conducted under these conditions produced the following results. With significantly different  $\tau_f$  values, the ‘true’  $T_1^{-1}$  rates for the methyls in question are 27 and 19 s<sup>-1</sup>. The spin diffusion causes partial averaging of the rates, resulting in  $T_{1,app}^{-1}$  of 24.5 and 21.5 s<sup>-1</sup>. This illustrates the pervasive character of deuterium spin diffusion in the experiments with sample spinning.

As always the case with spin-diffusion, any attempt at a truly quantitative description is predicated on the analysis of a very large spin network. In the context of the present experiment this is clearly not feasible. For each individual  $^2\text{H}$  spin the outcome will be dependent on the configuration of the surrounding spin network, the corresponding chemical shifts, and the intrinsic relaxation rates. Other factors can also play a role. For example, the initial conditions of the inversion-recovery experiment Fig. S2 are likely to be non-trivial. While  $^2\text{H}$  magnetization of the methyls is inverted reasonably well with a high-power 180° pulse, only partial inversion can be expected for other  $^2\text{H}$  sites where  $e^2qQ/h$  is not averaged by internal motion. Furthermore, slowly relaxing  $^2\text{H}$  spins are likely to become partially saturated during the measurement which uses relatively short interscan delays. As already mentioned, one should also consider the effect of proximal protons on  $^2\text{H}$ - $^2\text{H}$  spin diffusion. Thus, generally speaking, the problem is highly complex. Nonetheless, the above simplified analysis has demonstrated that the apparent  $T_1^{-1}$  relaxation rates for methyl  $^2\text{H}$  spins tend to be (i) lower than expected and (ii) more uniform than expected. The deviations from the true  $T_1^{-1}$  values are on the order of  $\geq 10\%$ , consistent with our experimental observations.

## References

1. Eichmüller, C.; Ryabov, Y.; Skrynnikov, N. R., to be published.
2. Scalley, M. L.; Yi, Q.; Gu, H. D.; McCormack, A.; Yates, J. R.; Baker, D., *Biochemistry* **1997**, *36*, (11), 3373-3382.
3. Phillips, J. C.; Braun, R.; Wang, W.; Gumbart, J.; Tajkhorshid, E.; Villa, E.; Chipot, C.; Skeel, R. D.; Kale, L.; Schulten, K., *J. Comput. Chem* **2005**, *26*, (16), 1781-1802.
4. Mittermaier, A.; Kay, L. E., *J. Am. Chem. Soc.* **1999**, *121*, (45), 10608-10613.
5. Chatfield, D. C.; Szabo, A.; Brooks, B. R., *J. Am. Chem. Soc.* **1998**, *120*, (21), 5301-5311.
6. Chatfield, D. C.; Augsten, A.; D'Cunha, C.; Wong, S. E., *J. Comput. Chem* **2003**, *24*, (9), 1052-1058.
7. Shaka, A. J.; Keeler, J.; Frenkiel, T.; Freeman, R., *J. Magn. Reson.* **1983**, *52*, (2), 335-338.
8. Metz, G.; Wu, X. L.; Smith, S. O., *J. Magn. Reson. Ser. A* **1994**, *110*, (2), 219-227.
9. Baldus, M.; Geurts, D. G.; Hediger, S.; Meier, B. H., *J. Magn. Reson. Ser. A* **1996**, *118*, (1), 140-144.
10. Marion, D.; Ikura, M.; Tschudin, R.; Bax, A., *J. Magn. Reson.* **1989**, *85*, (2), 393-399.
11. Pauli, J.; van Rossum, B.; Förster, H.; de Groot, H. J. M.; Oschkinat, H., *J. Magn. Reson.* **2000**, *143*, (2), 411-416.
12. Chevelkov, V.; Rehbein, K.; Diehl, A.; Reif, B., *Angew. Chem. Int. Ed.* **2006**, *45*, (23), 3878-3881.
13. Delaglio, F.; Grzesiek, S.; Vuister, G. W.; Zhu, G.; Pfeifer, J.; Bax, A., *J. Biomol. NMR* **1995**, *6*, (3), 277-293.
14. Clore, G. M.; Szabo, A.; Bax, A.; Kay, L. E.; Driscoll, P. C.; Gronenborn, A. M., *J. Am. Chem. Soc.* **1990**, *112*, (12), 4989-4991.
15. Skrynnikov, N. R.; Millet, O.; Kay, L. E., *J. Am. Chem. Soc.* **2002**, *124*, (22), 6449-6460.
16. Alla, M.; Eckman, R.; Pines, A., *Chem. Phys. Lett.* **1980**, *71*, (1), 148-151.
17. Gan, Z. H.; Robyr, P., *Mol. Phys.* **1998**, *95*, (6), 1143-1152. In Eq. (20) of this paper the matrix element (1,3) should read  $\sqrt{2}d_{12}^{(456)}$ , the matrix element (3,1) should read  $-\sqrt{2}d_{12}^{(456)}$ , and the matrix element (6,4) should read  $-\sqrt{2}d_{12}^{(456)}$ . In Fig. 2 of this paper the amplitude of  $\langle d_{12}^{(456)} \rangle$  should be approximately 2-fold lower than indicated in the plot. These corrections have been kindly confirmed by Dr. Zhehong Gan.
18. Doreleijers, J. F.; Mading, S.; Maziuk, D.; Sojourner, K.; Yin, L.; Zhu, J.; Markley, J. L.; Ulrich, E. L., *J. Biomol. NMR* **2003**, *26*, (2), 139-146.
19. Millet, O.; Muhandiram, D. R.; Skrynnikov, N. R.; Kay, L. E., *J. Am. Chem. Soc.* **2002**, *124*, (22), 6439-6448.
20. Fliege, J.; Maier, U., *IMA J. Numer. Anal.* **1999**, *19*, (2), 317-334.
21. Hologne, M.; Chen, Z. J.; Reif, B., *J. Magn. Reson.* **2006**, *179*, (1), 20-28.
22. Cavanagh, J.; Fairbrother, W. J.; Palmer, A. G.; Skelton, N. J., *Protein NMR Spectroscopy. Principles and Practice*. Academic Press Inc.: San Diego, 1996.
23. Ernst, M.; Meier, B. H., Spin diffusion. In *Solid-state NMR of polymers*, Ando, I.; Asakura, T., Eds. Elsevier: 1998; Vol. 84, pp 83-122.
24. Chevelkov, V.; Faelber, K.; Diehl, A.; Heinemann, U.; Oschkinat, H.; Reif, B., *J. Biomol. NMR* **2005**, *31*, (4), 295-310.